 doi:10.20944/preprints202105.0209.v1

Article

A multi scale minero-chemical analyses of biomass ashes: a key to evaluate their danger vs benefit.

Paola Comodi [1,*], Azzurra Zucchini [1], Umberto Susta [2], Costanza Cambi [1], Riccardo Vivani [3], Gianluca Cavalaglio [4], and Franco Cotana [4]

[1] Dipartimento di Fisica e Geologia, Università degli Studi di Perugia; paola.comodi@unipg.it, azzurra.zucchini@unipg.it, costanza.cambi@unipg.it
[2] UOC PSAL, AUSL Umbria 1; umberto.susta@uslumbria1.it
[3] Dipartimento di Scienze Farmaceutiche, Università degli Studi di Perugia; riccardo.vivani@unig.it
[4] Dipartimento di Ingegneria, Università degli Studi di Perugia; gianluca.cavalaglio@unipg.it, franco.cotana@unig.it
* Correspondence: paola.comodi@unipg.it

Abstract:

A multi-methodic analysis was performed on 5 samples of fly ashes coming from different biomasses. The aim of the study was to evaluate their possible re-use and their dangerousness for men and environment. Optical granulometric analyses indicate that the average diameter of the studied fly ashes is around 20 μm, whereas only ~1 vol% has diameter lower that 2.5 μm. The chemical composition, investigated with electron probe microanalysis, indicates that all the samples have a prevalent Ca composition, followed by Si and Al. A large content in K and P was observed in some samples, whereas the content in potentially toxic elements is always below the Italian law thresholds. Polycyclic aromatic hydrocarbons are completely absent in all the samples coming from combustion plants, whereas they are present in the fly ashes from the gasification center. Quantitative mineralogical content, determined by Rietveld analysis of X-ray powder diffraction data, indicates that all the samples have a large amorphous content, likely enriched in Ca, and several K and P minerals, such as sylvite and apatite. The results obtained from the performed chemo-mineralogical study allowed to point out that the biomass fly ashes could be interesting materials (1) as amending in clayey soils, in substitution to lime, to stimulating pozzolanic reaction and improve their geotechnical properties, on the one hand, avoiding to mine raw materials and, on the other hand, re-cycling wastes; (2) as agricultural fertilizes made by a new and ecological source of K and P.

Keywords: **biomass; fly ashes; X-ray diffraction; chemical analysis; multi-methodic analysis**

1. Introduction

Fly ashes represent the amount of the solid, inorganic residue left after the complete burning of the biomasses. They are an integral part of the plant materials and can have a wide range of elements. Due to the difference in raw materials as well as in the combustion plant type, the chemical physical characteristics of the flay ashes can be quite different [1]. Moreover, the percentage of ashes produced during biomasses burning varies according to the biomass type and ranging from a few units to about 10 dry weight percent [2,3].

Several papers [4,5,6] showed how the principal chemical components of biomass ashes are silicon, aluminum, calcium, iron, magnesium, sodium together with valuable amounts of important plant nutrients, such us potassium and phosphorous.

 doi:10.20944/preprints202105.0209.v1

The strong push towards the reuse of materials, together with the likely strong increase of fly ashes from biomass during the last decades, suggest the need to take actions devoted to their re-use as second generation products [7]. Important examples include agricultural, being biomass fly ashes used either as fertilizer or as raw materials to manufacture fertilizers, and concrete industry, where biomass fly ashes are used as an aggregate/binder in concrete production [8 and references therein] contributing to enhance the sustainability of the concrete industry. In particular, biomasses ashes, e.g., from sugar can bagasse, forest residues, wheat straw, can be added to concrete as relevant components due to their pozzolanic properties [9,10,11, 12].

On the other hand, they can be used for producing silicon-based materials because of their very high silica content or in the soil stabilization management [13,14].

Due to their broad range of features, the identification of the beneficial re-use passed through the detailed characterization of the biomass fly ashes. The chemical composition of as usually represented by the macro elements Ca, K, P and S, which suggests the possibility of their agricultural use [15] but they can contain heavy metals [16] as well as polycyclic aromatic hydrocarbons (PAH) that can be produced by the thermal decomposition of organic matter, due to incomplete combustion, e.g., either in engines and incinerators or when biomass burns in forest fires. Domestic wood burning and road traffic are the major sources of PAHs [17].

These components can hinder their use, due to their the cancerogenic character [18] and should be monitored before being reused in a sustainable way directly either as fertilizer or raw material to manufacture fertilizers and returned to soils.

Cabrera et al. [11] characterized the biomass performances (energetic, physical, and chemical) of different biomass feedstocks: the lignocellulosic residues of cardoon energy crop, the pruning of grapevine and olive trees and the residues from the river maintenance (turkey oak). Each biomass sample was characterized in terms of moisture content, ashes content, volatile substances, fixed carbon, low and high heating value [19], content of carbon, nitrogen, hydrogen and main metals [20]

This paper intends to study, with a multi methodic approach, a group of ashes products from different biomasses and from different combustion plants. Some of these samples are the same already characterized in [3] and allow us to relate the characteristics of raw materials with those of ashes. In addition, a sample from a gasification plant and a sample from pellet combustions, were investigated.

The samples were characterized from a morphological, chemical and mineralogical point a view. In particular, granulometric analysis was performed by diffraction light scattering and optical analysis, to determine the amount of PM10 and PM2.5 fraction which can impact on the air pollution [21]; X-ray powder diffraction (XRPD) analysis to determine the amount of amorphous component as well the crystalline fraction, to define in which form the chemical component are allocated and to define their availability and solubility for agricultural and/or other employs; thermal analyses (TA) to investigated the loss of mass during heating cycles and to determine the amount of volatile components. Moreover, bulk chemical analysis of major, minor and trace elements (in particular heavy metals and potentially toxic elements, PTE) were determined by means of electron microprobe coupled with wavelength dispersive spectroscopy (EMPA – WDS) technique. Field emission scanning electron microscopy (FE-SEM), coupled with microanalysis (energy dispersive spectroscopy – EDS), was used to investigated the micro-textural characteristic, especially focused on the analysis of the possible occurrence of either concentric or zoned element distributions. Lastly, gas-chromatography technique was used to determine PAH contents.

2. Materials and Methods

2.1 Samples

Preprints (www.preprints.org) | NOT PEER-REVIEWED | Posted: 10 May 2021 doi:10.20944/preprints202105.0209.v1

The type and the origin of samples investigated in this study are reported in table 1

Table 1. Samples used in the present work.

Code	Type	Origin
#1	Biomass ashes	Gasification power plant, Magione (PG) Italy
#2	Biomass ashes	Grapevine prunings, Torgiano (PG) Italy
#3	Biomass ashes	Wood pellet
#4	Biomass ashes	Olive tree prunings
#5	Biomass ashes	Cardoon plants

2.2 Experimental thecniques

2.2.1 XRPD analyses

X-Ray Powder Diffraction analyses were performed on randomly oriented powder, at room temperature, using a Phillips PW-1830 with CuKα radiation ($\lambda = 1.5406$). The device was equipped with a graphite monochromator. The voltage and current intensity of the generator were set at 40 kV and 30mA. The acquisition step size corresponds to 0.3° and the step time equals 18 s. All the acquired diffraction patterns were collected in a Bragg-Brentano geometry (θ-2θ), in a range of 2θ extending from 5° to 80°. The quantitative interpretation of the of the samples mineralogical composition was performed applying the Rietveld method [22] as implemented in GSAS – EXPGUI [23,24]. Background was fitted with a Chebyshev polynomial function and diffraction patterns were modeled by a pseudo-Voight function with one Gaussian and one Lorentzian coefficient. Scale factor, lattice constants and profile coefficients were refined for each phase. Crystalline silicon (Si) was added as external standard (10% by weight) for the calculation of the amorphous content.

2.2.2 TGA-DTA analyses

Thermogravimetric analyses (TGA) were performed with a Netzsch STA 449F3. Approximately 50 to 100 mg of finely ground material was heated at a rate of 10°C min^{-1}, under room atmosphere, from 20 up to 1000 °C. The Netzsch software was used to process the results at Department of Chemistry of Perugia University, Italy.

Differential Thermal Analysis (DTA) is a thermal analysis technique in which the heat flow into or out of a sample is measured as a function of temperature or time, while the sample is exposed to a controlled temperature program [25]. It is a very powerful technique to evaluate material properties such as glass transition temperature, melting, crystallization, specific heat capacity, cure process, purity, oxidation behavior, and thermal stability.

2.2.3 SEM analyses

The surface morphology and the chemical composition were examined through Field Emission - Scanning Electron Microscopy (FE-SEM) by using a LEO 1525 with a ZEISS AsB (Angle selective backscattered, Oberkochen, Germany) detector, available at the Department of Physics and Geology of the University of Perugia. The FE-SEM instrument was coupled with EDS microanalysis (BrukerQuantax EDS). Gold coating was applied for SEM observations.

2.2.4 Granulometric analysis

The particle sizes, with dimension over 3 microns were determined by using and Accusizer TM Optical Particle Sizer Model 770 (Santa Barbara, California, USA), whereas for particle size lower than 3 microns the dynamic light scattering technique was employed by using a NICOMP 380 ZLS zeta potential/particle sizer (PSS NICOMP; Santa

Preprints (www.preprints.org) | NOT PEER-REVIEWED | Posted: 10 May 2021 doi:10.20944/preprints202105.0209.v1

Barbara, USA). Approximately 10 mg of each sample was dispersed in 1 ml of bi-distilled water and sonicated for 10 sec to improve the dispersion of the single particles.

2.2.5 EMPA analysis

The samples were also analyzed in terms of bulk composition. In order to obtain homogeneous pellets, the ashes were heat treated up to and beyond their fusion points. The heating was performed by putting few grams of each specimen into a crucible made out of pure Pt and using a muffle capable of 1600°C. Once the samples were completely molten, they were quickly quenched at room temperature. The glass pellets obtained after the quenching were embedded with epoxy resin; the mounts were cut, ground and highly polished down to a 1 μm grade diamond polishing paste.

Before being analyzed, each polished mount had to be coated using graphite. EMPA–WDS analyses were carried out at the Electron Microprobe Laboratory of Earth Science Department "Ardito Desio" (University of Milan, Italy) using the EMPA–WDS JEOL 8200 Super Probe with 5 WDS channels and one EDS cannel under the following operating conditions: accelerating voltage, 15 kV; beam current, 5 nA; counting time, 30 seconds for all the elements and 10 seconds for the backgrounds. Calibration for chemical analysis was accomplished with a set of synthetic and natural standards, including: grossular (Al, Si, Ca), omphacite (Na), olivine (Mg), apatite (P), scapolite (Cl), pure Cr, rhodonite (Mn), fayalite (Fe), K-feldspar (K) and ilmenite (Ti).

2.2.6 PAH (polycyclic aromatic hydrocarbons)

To evaluate the possible dangerous character of fly ashes and to determine their possible employments, the polycyclic aromatic hydrocarbons measurements were performed.
The samples were analyzed with gas chromatography (Agilent mod. 6890) coupled with mass spectrometry (5973N di Agilent Technologies), by using reference standards.
The total amount of PAH, including naftalene, acenaftene, acenaftilene, fluorene, fenatrene, antracene, fluoratene, pirene, benzoantracene crysene, benzo(b,k,j) fluorantene, benzo(e)pirene, benzo(a)pirene, indenopirene, dibenzo(a,h)antracene, benzo(g,h,i)perilene, was determined.

3. Results

3.1 Granulometric results

The results of granulometric analysis are reported in Figure 1. The average sizes are quite similar for the 5 samples and equal to 23.8, 17.0, 21.0, 21.0, 18 μm from sample 1 to 5.

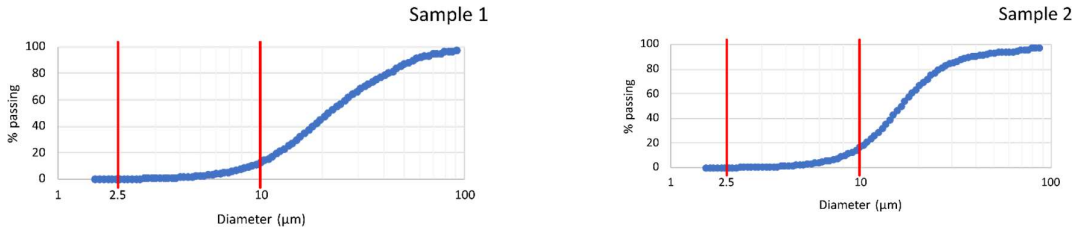

(a) (b)

Preprints (www.preprints.org) | NOT PEER-REVIEWED | Posted: 10 May 2021 doi:10.20944/preprints202105.0209.v1

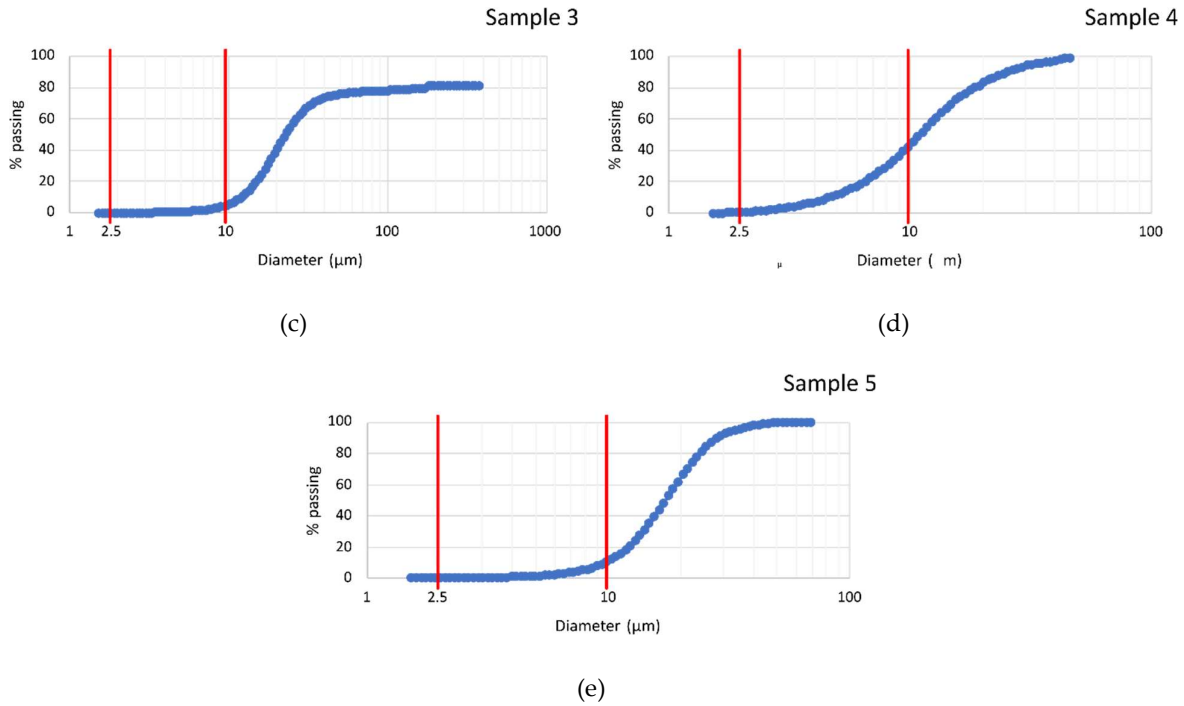

Figure 1 Grain size distribution for the 5 samples determined by dynamic light scattering. Samples from 1 to 5 are shown from (a) to (e). The vertical red lines highlight the 10- and 2.5-micron diameters.

On the other hand, more relevant differences can be evidenced from the analysis of the granulometric curves reported in Figure 1 where the red lines highlight the position of the 2.5 and 10 µm diameter particles. These values represent important limits as they discriminate the inhalation properties and, thus, the health hazard for their inhalation capacities.

All samples contain very low percentage of particles with dimension under 2.5 µm (less than 1vol%); whereas, the content in particles with diameter less than 10 µm is quite different, varying from 5vol% in sample 5 to 40vol% in sample 4.

3.2 X-ray diffraction results

The quantitative mineralogical composition as well the amount of amorphous component is reported in Table 2, whereas Figure 2 shows the X-ray diffraction profiles collected and calculated with Rietveld analyses. In particular, in the graphs, the red crosses represent the data collected, the green lines the calculated best-fitting profiles, obtained adding in the refinements the minerals reported in Table 2. The theoretical peaks position of each mineral is reported under the profile, i.e., each horizontal line with different bars represents the theoretical peak position for that mineral. The lowest bar line reports the theoretical peck position of metallic Si, added to each sample as internal standard, for the quantitative analysis. The pink profile in the lower part of each graph represents the difference profile generated subtracting the measured profile to the calculated one.

Preprints (www.preprints.org) | NOT PEER-REVIEWED | Posted: 10 May 2021 doi:10.20944/preprints202105.0209.v1

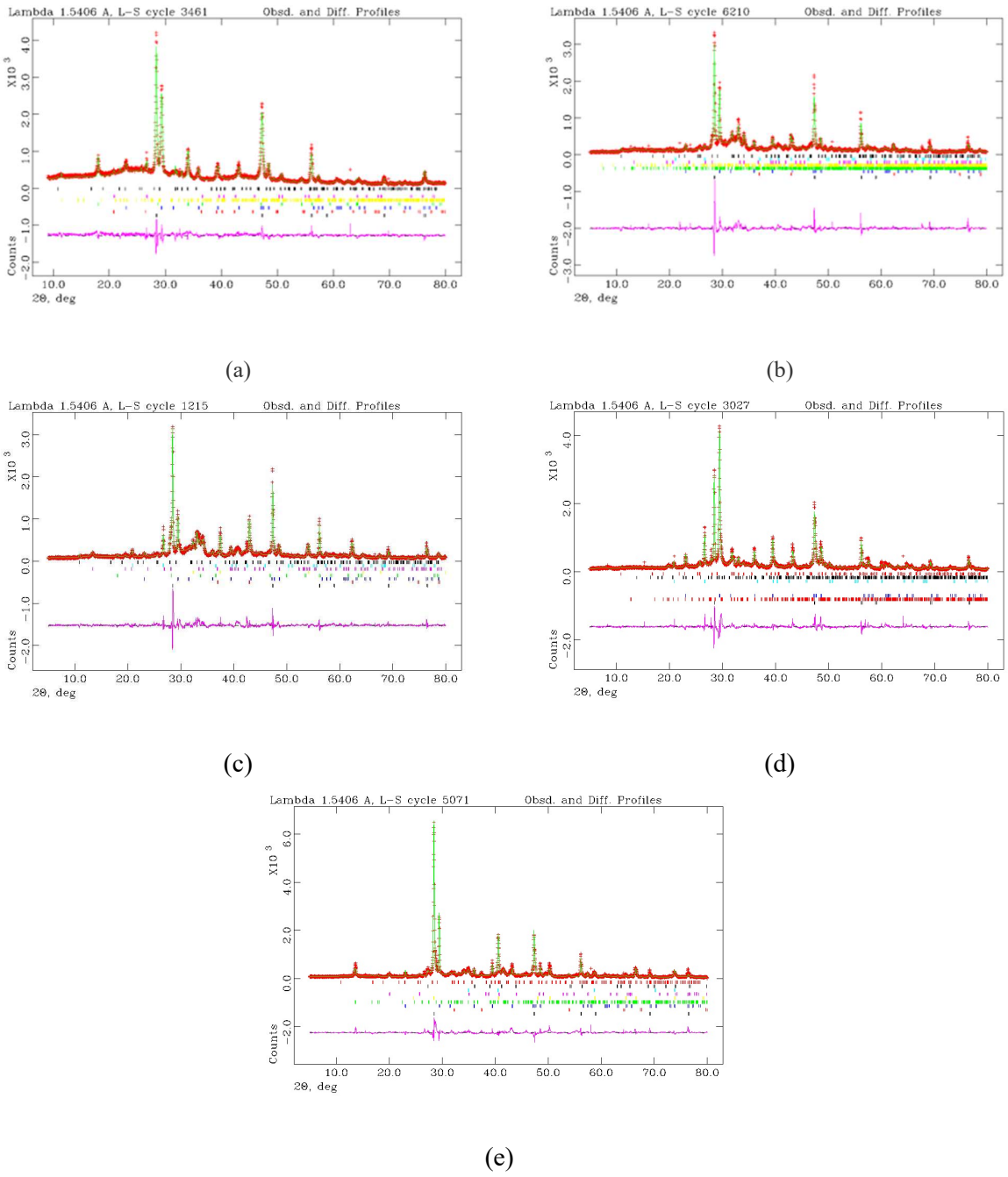

Figure 2. XRPD patterns refined by means of the Rietveld method for samples #1 (a), #2 (b), #3 (c), #4 (d) and #5 (e). Observed and calculated profiles are given in red and green, respectively. The difference between the observed and calculated powder diffraction profiles is in purple. Thick marks below the diffractograms are the diffraction peaks positions per each phase.

Table 2 Quantitative analysis by Rietveld refinement of XRPD data. Quantitative results are given in wt%. Errors on wt% are also listed. Amorphous is recalculated based on Si as external standard.

Preprints (www.preprints.org) | NOT PEER-REVIEWED | Posted: 10 May 2021 doi:10.20944/preprints202105.0209.v1

Sample	Phases	Chemical formula	wt%	error
#1	Quartz	SiO_2	2,91	0,01
	Calcite	$CaCO_3$	21,01	0,07
	Portlandite	$CaO(OH)_2$	4,47	0,05
	Sulphur	S	0,41	0,02
	Hydroxylapatite	$Ca_5(PO_4)_3(OH)$	3,11	0,02
	Amorphous		68.1	0.1
#2	Periclase	MgO	1,81	0,01
	Calcite	$CaCO_3$	8,34	0,04
	Heulandite	$(Ca,Na)_{2-3}Al_3(Al,Si)_2Si_{13}O_{36}\bullet 12(H_2O)$	1,15	0,03
	Calcioferrite	$Ca_4Fe^{2+}(Fe^{3+},Al)_4(PO_4)_6(OH)_4\bullet 12(H_2O)$	1,60	0,02
	Fairchildite	$K_2Ca(CO_3)_2$	2,23	0,01
	Quartz	SiO_2	0,33	0,11
	Hydroxylapatite	$Ca_5(PO_4)_3(OH)$	5,08	0,21
	Amorphous		79,5	0.2
#3	Periclase	MgO	5,77	0,02
	Calcite	$CaCO_3$	6,36	0,05
	Portlandite	$Ca(OH)_2$	0,63	0,04
	Lime	CaO	2,06	0,02
	Fairchildite	$K_2Ca(CO_3)_2$	11,20	0,03
	Quartz	SiO_2	0,52	0,14
	Apatite	$Ca_5(PO_4)_3(OH,F,Cl)$	1,39	0,26
	Amorphous		72.1	0.3
#4	Reichenbachite	$Cu^{2+}{}_5(PO_4)_2(OH)_4$	0,95	0,02
	Calcite	$CaCO_3$	42,24	0,15
	Quartz	SiO_2	4,18	0,07
	Phosphoferrite	$(Fe^{2+},Mn)_3(PO_4)_2\bullet 3(H_2O)$	0,42	0,03
	Hydrossilapatite	$Ca_5(PO_4)_3(OH)$	4,57	0,03
	Amorphous		47.6	0.5
#5	Lime	CaO	0,08	0,01
	Calcite	$CaCO_3$	6,62	0,03
	Fluellite	$Al_2(PO_4)F_2(OH)\bullet 7(H_2O)$	3,48	0,03
	Sylvite	KCl	2,99	0,01
	Quartz	SiO_2	0,28	0,01
	Rhodochrosite	$MnCO_3$	0,51	0,09
	Rutile	TiO_2	0,16	0,18
	Hydroxilapatite	$Ca_5(PO_4)_3(OH)$	1,13	0,26
	Amorphous		84.7	0.3

3.3 Thermal analysis results

The thermal analysis of the 5 investigated samples shows relevant differences on the weight losses. Results are given in Figure 3.

The first steps in TG at approximately 100 °C, with weigh losses between 1 to 18 wt%, observed in all the samples excluding sample #5 correspond to endothermic peaks in DTA (Figure 4) and can be associated to the loss of hygroscopic water, absorbed after the combustion of oxides. In the sample #1 at approximately 400 °C, where there is a weigh loss of about 50 wt%, corresponding in the DTA spectra at an exothermic peak, and associated to the combustion of residual organic matter.

The step at approximately 600 °C can be related either to the well-known carbonate decomposition reaction ($CaCO_3$ to $CaO + CO_2$), or to the decomposition of calcium-phosphates ($Ca_3(PO_4)_2 = CaO + P_2O_5$ or $K_3PO_4 = 3K_2O + P_2O_5$) where the phosphorous pentoxide is lost as gas.

Preprints (www.preprints.org) | NOT PEER-REVIEWED | Posted: 10 May 2021 doi:10.20944/preprints202105.0209.v1

On the whole the total mass losses between 20 and 1200 C varies from 13.38 in the sample #2 to 70.84 in the sample #1,

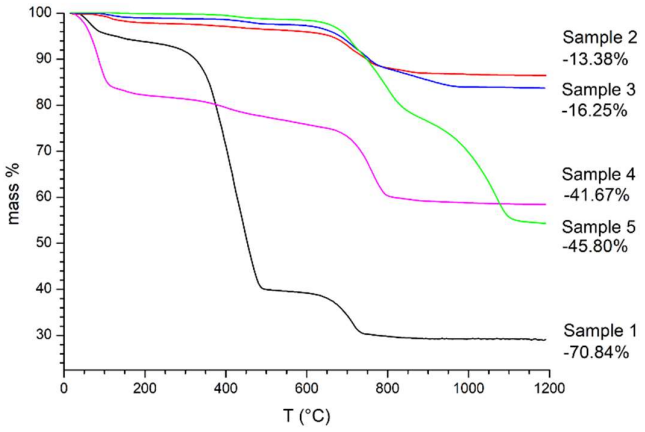

Figure 3. TGA thermal gravimetric analyses for the 5 sample of the biomass fly ashes studied.

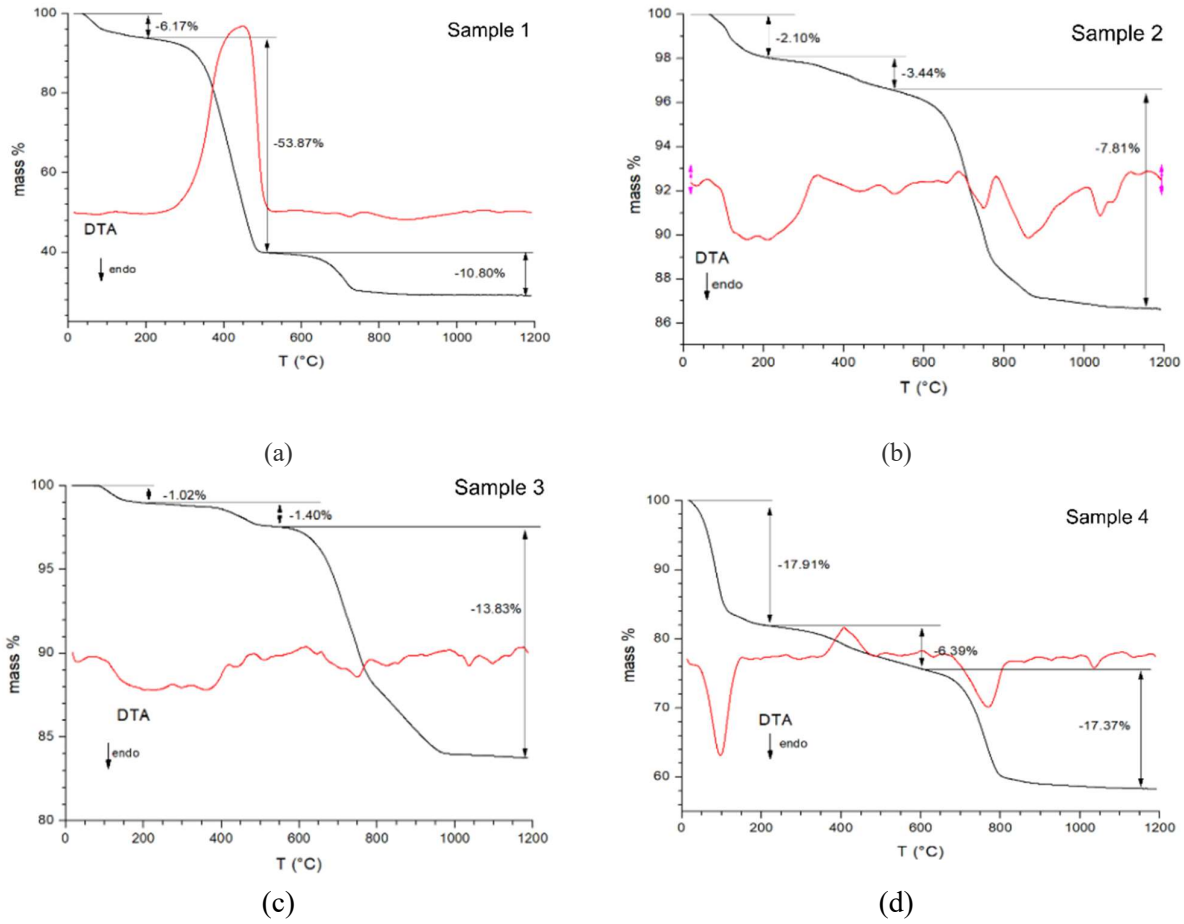

Preprints (www.preprints.org) | NOT PEER-REVIEWED | Posted: 10 May 2021 doi:10.20944/preprints202105.0209.v1

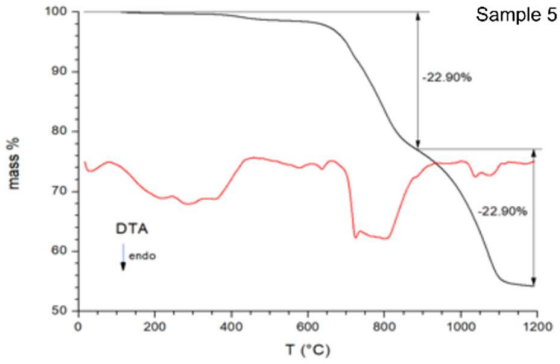

(e)

Figure 4. Thermal gravimetric analyses (TGA) in black and Differential Thermal Analysis (DTA) in red for the 5 analyzed fly ashes: #1 (a), #2 (b), #3 (c), #4 (d) and #5 (e).

3.4 Electron microscopy results

Results of FE-SEM analysis coupled with EDS semi-quantitative chemical analysis are shown in Figures from 5 to 8 where interesting textural features are shown together with some of the accessory minerals also found by XRPD analysis. Apatite crystals appear as roundly shaped at sub-micrometric to deci-micrometric size (apatite in samples #2 and #5, Figure 5 and Figure 7). Moreover, elongated K_2O and KCl crystal are shown in sample # 4 and sample #5 (Figures 6 and Figures 7).

Interesting de-vitrification microstructures are also observed in sample #3 (Figure 8). In particular, windmill structures and neoblasts surrounded by glass are shown.

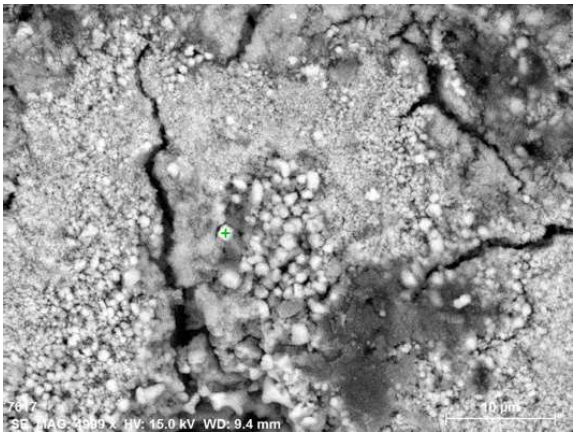

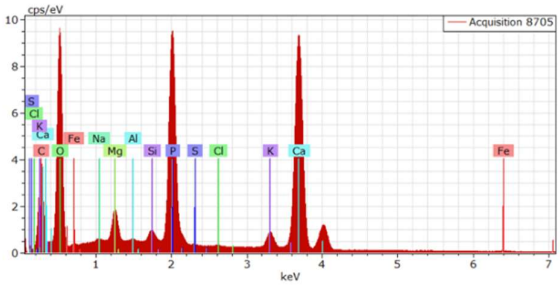

(a) (b)

Figure 5. FE-SEM analysis of sample #2. On the left (a), a secondary electron (SE) image where micrometric sub-spherical crystals of apatite are shown. On the right (b), the graph reports the EDS analysis collected in the apatite crystal at the point indicated with the green cross.

Preprints (www.preprints.org) | NOT PEER-REVIEWED | Posted: 10 May 2021 doi:10.20944/preprints202105.0209.v1

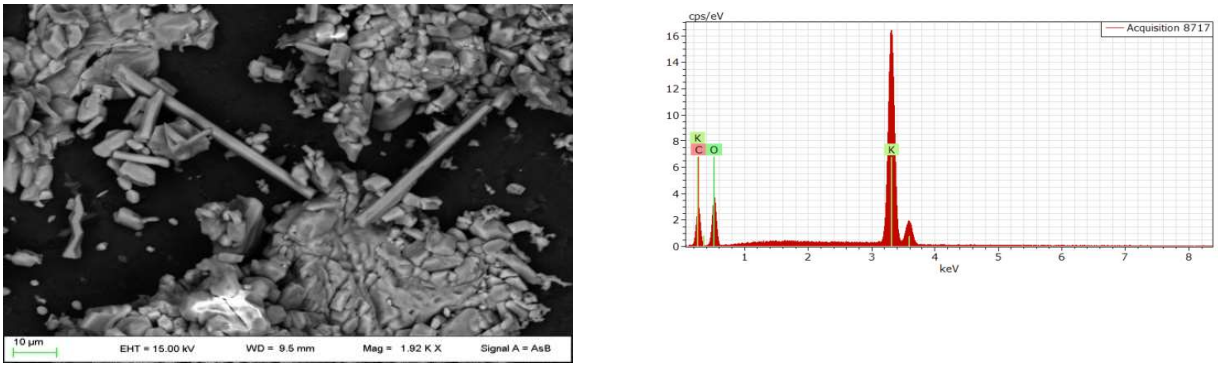

(a) (b)

Figure 6. FE-SEM analysis of sample #4. On the left (a), a SE image with elongated K_2O crystals. On the right (b), the EDS data collected in one of the elongated crystals is shown.

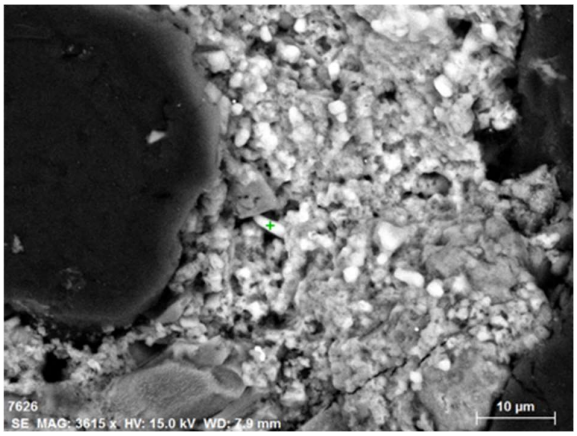

(a)

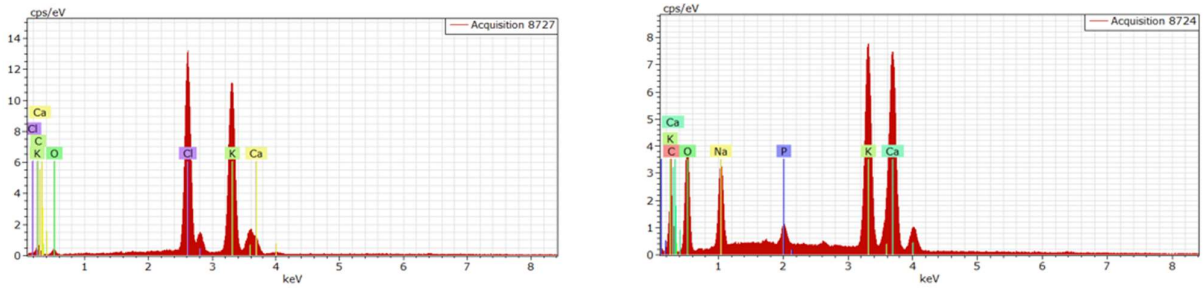

(b) (c)

Figure 7. FE-SEM analysis of sample #5. On the left (a), a SE image where elongated and rounded crystals are shown. In (b) and (c), the graphs report the EDS spectra collected in one of the elongated crystals (sylvite, KCl) and in the rounded crystals [apatite, crystals $Ca_5(PO_4)_3(F, OH, Cl)$], respectively.

Preprints (www.preprints.org) | NOT PEER-REVIEWED | Posted: 10 May 2021 doi:10.20944/preprints202105.0209.v1

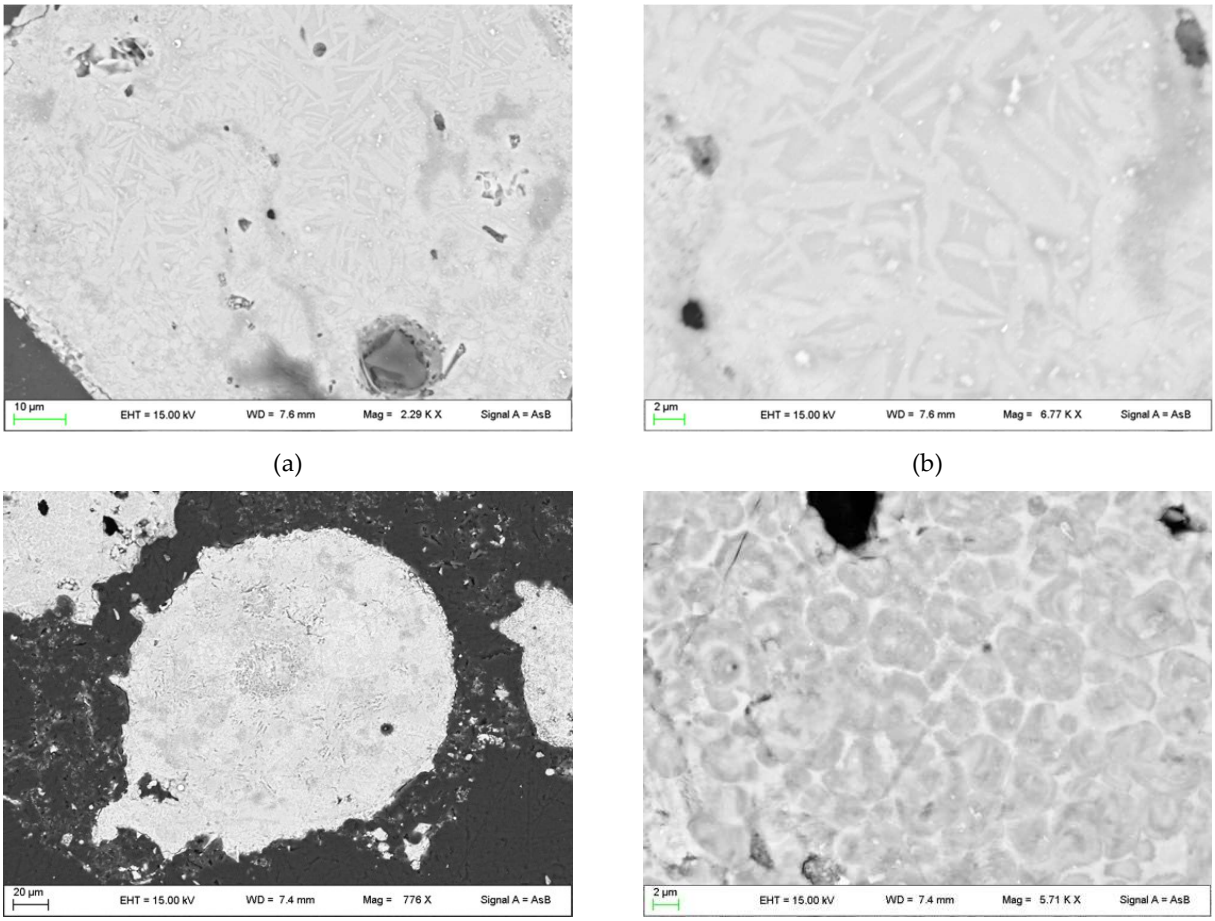

Figure 8. De-vetrification microstructures observed in sample #3. In (a) and (b) two different magnification of windmill structures are reported; whereas in (c) and (d) two different SE imagines at different magnification on microstructures showing neoblasts surrounded by glass.

3.5 Chemical composition results

The chemical analysis of the major elements in the studied fly ashes (Table 3) indicated that the main component for all of them is CaO, followed by SiO_2 and then by Al_2O_3 or in one case by MgO. The component P_2O_5 is dominant for sample 2 reaching approximately 9 wt%, whereas for sample 4 the concentration of K_2O reaches 4 wt%.

These data fit well with FE – SEM – EDS microanalysis, where several apatite microcrystals were found in sample 2 (Figure 5) and elongated crystal of K_2O in sample 4 (Figure 6).

Table 3. Major elements (in wt% oxides) measured with EMPA in the 5 samples

Sample	#1	#2	#3	#4	#5
NaO	0.08	0.94	0.112	0.582	0.907
Cl	0.30	0.009	0.008	0.006	0.008
MnO	0.146	0.127	1.113	0.121	0.025
K_2O	0.184	1.78	0.005	4.944	0.008
MgO	0.213	9.143	32.39	3.854	1.563

Preprints (www.preprints.org) | NOT PEER-REVIEWED | Posted: 10 May 2021 doi:10.20944/preprints202105.0209.v1

SiO_2	11.76	26.19	16.512	27.949	9.567
Cr_2O_3	0.136	0.0186	0.007	0.014	0.007
FeO	0.611	2.34	2.765	2.889	0.537
CaO	39.84	44.26	37.215	43.31	65.042
Al_2O_3	0.55	5.52	5.540	7.907	1.103
P_2O_5	0.392	8.856	3.508	7.832	7.677
TiO_2	0.067	0.318	0.202	0.349	0.084
Total	54.28	99.515	99.375	99.760	86.53

Table 4. Minor elements (ppm) for the 4 samples, measured with EMPA in the 4 samples (#2, #3, #4 and #5)

Sample	#2	#3	#4	#5
V	33.44	32.07	54.08	7.08
Cr	0.13	43.44	0.13	13.55
Co	8.38	22.92	8.44	3.09
Ni	59.40	191.00	51.30	22.18
Zn	479.20	85.20	114.96	51.30
Pb	0.22	0.53	0.13	0.52
Cu	304.62	17.36	153.38	7.85
As	0.25	3.05	0.51	2.21
Cd	0.05	0.23	0.02	0.71
Hg	0.00	0.00	0.00	0.00
Se	0.00	0.00	0.00	0.32
Mo	0.59	184.37	0.23	37.28
Cl	117.40	159.33	97.20	147.80
S	498.63	573.00	314.50	382.00

Potentially Toxic Elements (PTE), namely As, Cd, Cr, Cu, F, Pb, Hg, Mo, Ni, Se, V, Zn are naturally present in the environment [26], and some of them, in low percentage, can be essential for the correct metabolism of biologic activity. However, when their concentration increases, they can become toxic. Their accumulation can be caused by the anthropogenic activities such as mining, industrial and agricultural activities [27] and is dependent on their mobility. For most of the PTEs, the mobility increases with the decrease in pH, very rapidly at pH lesser than 7, whereas at higher pH conditions it slows down. Beyond pH, other soil parameters, including organic matter (OM), redox considerations, chemistry of soil particles and composition of clay, affect the distribution, concentration and mobility of PTEs. They are considered as hazardous contaminants due to their ability to intoxicate, be aggregated and be persistent in the environmental media. For these reasons, several legislative decrees (for Italy is n° 152/2006) define the concentration limits for PTE in urban and industrial areas.

The chemical analyses of PTE are listed in Table 4 for samples #1, #3, #4 and #5. As for sample #1, it was impossible to be homogenized as it burned during annealing even before melting. In Figure 9 the value of some selected PTEs (V, Cr, Co, Ni, Zn, Pb, Cu, As, Hg, Se), together with Cl and S, are reported, as measured in the four analyzed samples of fly ashes.

The comparison of the measured concentration for PTEs with the Italian limits for urban and industrial sites are shown in Figures 10 and 11, respectively. All samples have PTE concentration below the legislative limit for the industrial site and only sample #2 have Cu and Zn, and for sample #4 for Cu, that have values above the legislative limits.

Preprints (www.preprints.org) | NOT PEER-REVIEWED | Posted: 10 May 2021 doi:10.20944/preprints202105.0209.v1

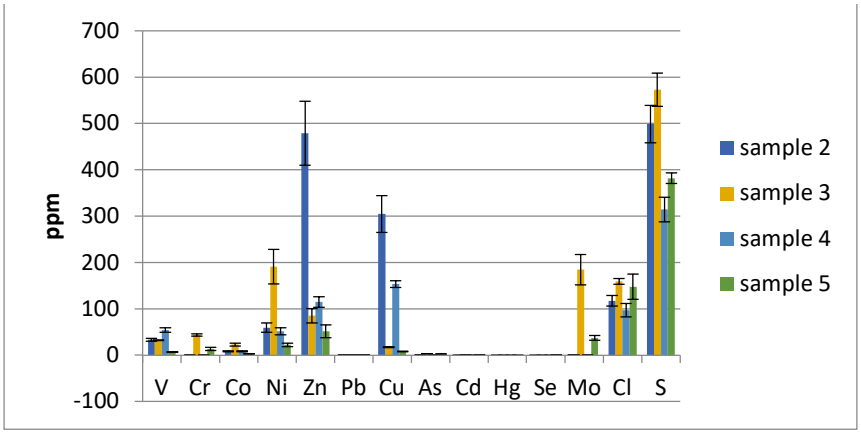

Figure 9. Selected PTEs (V, Cr, Co, Ni, Zn, Pb, Cu, As, Hg, Se), Cl and S concentration in the four samples with potentially toxic elements.

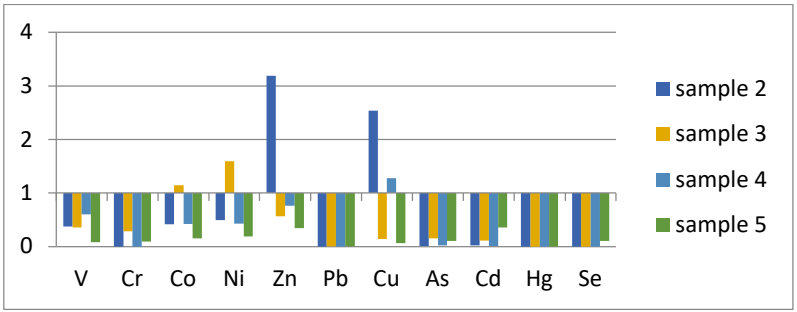

Figure 10. Comparison of the measured concentration for V, Cr, Co, Ni, Zn, Pb, Cu, As, Hg, Se, with the Italian limits for urban sites.

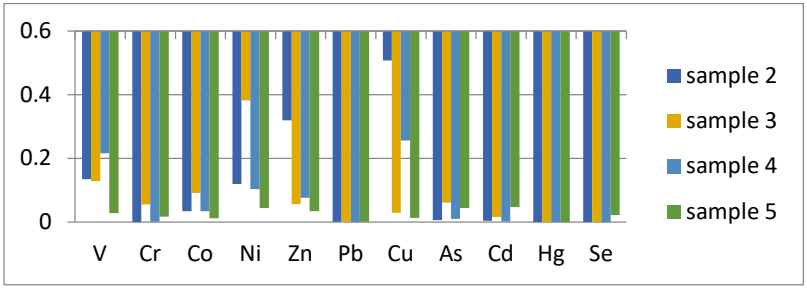

Figure 11. Comparison of the measured concentration for V, Cr, Co, Ni, Zn, Pb, Cu, As, Hg, Se, with the Italian limits for industrial sites.

The total amount of PAH, naftalene, acenaftene, acenaftilene, fluorene, fenatrene, antracene, fluoratene, pirene, benzoantracene crysene, benzo(b,k,j) fluorantene, benzo(e)pirene, benzo(a)pirene, indenopirene, dibenzo(a,h)antracene, benzo(g,h,i)perilene, (Table 5) are below the detection limits for all the investigated samples, with the exception of sample 1, from gasification plants.

Table 5. PAH content in the 5 samples investigates in the present work. Data are given in mg/kg t.q.

PAH type/samples	1	2	3	4	5
Total IPA	1088	<0.050	<0.050	<0.050	<0.050

Preprints (www.preprints.org) | NOT PEER-REVIEWED | Posted: 10 May 2021 doi:10.20944/preprints202105.0209.v1

Naftalene	3706	<0.010	<0.010	<0.010	<0.010
Acenaftene	4.6	<0.010	<0.010	<0.010	<0.010
Acenaftilene	341	<0.010	<0.010	<0.010	<0.010
Fluorene	<0.010	<0.010	<0.010	<0.010	<0.010
Fenantrene	29	<0.010	<0.010	<0.010	<0.010
Antracene	4.0	<0.010	<0.010	<0.010	<0.010
Fluorantene	1.6	<0.010	<0.010	<0.010	<0.010
Pirene	1.3	<0.010	<0.010	<0.010	<0.010
Benzo(a)antracene	0.015	<0.010	<0.010	<0.010	<0.010
Crysene	0.020	<0.010	<0.010	<0.010	<0.010
Benzo(b,k,j)fluorantene	<0.010	<0.010	<0.010	<0.010	<0.010
Benzo(e)pirene	<0.010	<0.010	<0.010	<0.010	<0.010
Benzo(a)pirene	<0.010	<0.010	<0.010	<0.010	<0.010
Indenopirene	<0.010	<0.010	<0.010	<0.010	<0.010
Dibenzo(a,h)antracene	<0.010	<0.010	<0.010	<0.010	<0.010
Benzo(g,h,i)perilene	<0.010	<0.010	<0.010	<0.010	<0.010

4. Discussion

The comparison of the multimethodological analyses here performed on five samples coming from fly ashes of different vegetal biomasses, allows to make the following considerations:

1. The PTE concentrations were evaluated for the human and ecological potential risk, since their accumulation increases the toxic hazard [29]. In all of the samples of fly ashes from biomasses, the PTE analyzed are below the limit indicated from Italian legislation. Moreover, the PAH content is undetectable for all sample with the exception of sample #1, which is the unique samples coming from a gasification plant.
   Gasification is a process that converts either biomass [30] or fossil fuel-based carbonaceous materials, into gases. The process consists in the reaction of the feedstock material, at high temperatures (typically > 700 °C) without combustion, via controlling the amount of oxygen and/or steam present in the reaction. The resulting gas mixture is called syngas (from synthesis gas) or producer gas and its largest fraction is made by nitrogen (N_2), carbon monoxide (CO), hydrogen (H_2), and carbon dioxide (CO_2). Due to the flammability properties of the H_2 and CO, syngas is itself a fuel.
   The thermal analysis performed in this work showed a strong weight loss, more that 50wt%, at approximately 400°C for the sample #1. Indeed, during the process, some material can remain un-combusted likely due to the large amount of PAH content in that sample.

2. The granulometric analysis indicates that the PM2.5 fraction, namely the amount of particle with an average dimension below 2.5 μm, which can represent a danger to human health, due to their hinalability, is quite lower than 1%; whereas, the content in particles with diameter less than 10 μm is quite different, varying from 5% in sample #5 to 40% in sample #4.

3. The high content in phosphorous, as apatite mineral, as well as in potassium, as sylvite mineral, suggests that these materials can represent a good amending for agricultural lands, once the bioavailability of these elements can be proved and verified. The electron microscopy analysis showed that usually the crystals have very low dimensions, from nanometer scale to few microns. Moreover, the Rietveld analysis indicated that the amorphous content in all samples is very high from 47.6 wt% in sample #1 up to 84.7 wt% in the sample #5. Both the above-mentioned characteristics are

 doi:10.20944/preprints202105.0209.v1

a good indicator of a large reaction surface, one the most important parameter for bioavailability.

4. The high Ca content revealed in the analyzed samples by the chemical analysis has not a counterpart in the mineralogical composition of the samples as relevant amount of Ca-minerals were not observed by XRPD data processing. Thus, the high Ca content is supposed to be stored in the amorphous phase, that is quite abundant in the studied fly ashes.

5. The high Ca content measured in the samples, suggests that these materials can be used as amending in soils, usually clayey soils, with low geotechnical properties. In these soils, the traditional addition of CaO coming from the decarbonation reaction of carbonate minerals, improves the mechanical properties as pozzolanic reactions induced by the highly alkaline environment promote the formation of new binding compounds such as calcium-silicate-hydrated minerals (C-A-H; C-S-H) [31,32,33]. In a high pH environment, natural pozzolanas, rich in silicon and amorphous phase, promote pozzolanic reactions as they increase the availability of silicon and alumina [34]. The large amount of amorphous content, evidenced from Rietveld analysis, and the chemical compositions of the analyzed ashes samples, suggest that, at least some of them, could be successfully used, in combination or substitution of traditional binders, in soil stabilization. Such use would require the environment to reach the alkalinity needed to promote pozzolanic reactions, with or without the addition of alkaline activators, normally used for soil treatment by means of fly ashes [34].

Conclusions

The addition of Ca from fly ashes in soil with poor geotechnical properties can represent a good example of end of wastes. In fact, in this way, two waste materials, namely fly ashes and clayey soils, can be reconverted in a good second-generation product, thus avoiding the removal and transport of the soils, the opening of new caves to the extraction of carbonate, and reducing the CO_2 emission from transports and de-carbonatation reaction.

The present study indicates that the dimension and the chemical composition of the studied fly ashes, namely the low content of PTEs and PAH (with the exception of sample from gasification plant), as well as the high CaO content in the amorphous fraction, represent favorable factors that enhance the interest in the applicability areas of these products. The biomass fly ashes, in fact, could be used as amending in clayey soils in substitution to lime, to stimulate pozzolanic reactions and improve their geotechnical properties. Further experiments to check the effect of the addition of fly ashes with high CaO content in clayey soils are in progress.

Moreover, the application of fertilizer P in intensive crop and animal production systems has increased pressure on finite global reserves of phosphate rocks [35], and their availability worldwide has recently highlighted important criticisms, due to both the strong depletion of natural reserves and their geo-localization in limited areas.

Biomass fly ashes showed a high phosphorous and potassium content, present in nano-micro crystals (as electron microscopy evidenced) that biomass have assimilated during their life cycle. The possibility that biomass fly ashes could be used as agricultural fertilizes, opens an interesting perspective to have a new and ecological source of K and P.

The above-mentioned scenarios fit well in the principles of circular economy, where waste materials, such as the biomass fly ashes, are re-cycled and used as a second-generation product, avoiding to mine natural raw materials, such as carbonated and phosphate rocks.

 doi:10.20944/preprints202105.0209.v1

Author Contributions: "Conceptualization, P.C., F.C., G.C.; methodology, P.C., A.Z., U.S., G.C., R.V. C.C.; validation, A.Z., U.S., P.C.; resources, P.C.; data curation, P.C., A.Z., U.S., G.C., R.V, P.C., A.Z., C.C.; funding acquisition, P.C. All authors have read and agreed to the published version of the manuscript."

Funding: "This research was founded by Fondazione Cassa di Risparmio di Perugia (Italy) with title: Ceneri da biomassa e da carbone: possibili reimpieghi e strategie di bonifica. Project number: #2018.0508

References

1. Torquati, B.; Marino, D.; Venanzi, S.; Porceddu, P.; Chiorri, M. Using tree crop pruning residues for energy purposes: A spatial analysis and an evaluation of the economic and environmental sustainability. *Biomass Bioenergy* **2016**, *95*, 124–131.
2. James, A.K.; Thring, R.W.; Helle, S.; Ghuman, H.S. Ash Management Review—Applications of Biomass Bottom Ash. *Energies* **2012**, *5*, 3856–3873.
3. Cavalaglio, G.; Cotana, F.; Nicolini, A.; Coccia, V.; Petrozzi, A.; Formica, A.; Bertini A. Characterization of Various Biomass Feedstock Suitable for Small-Scale Energy Plants as Preliminary Activity of Biocheaper Project. *Sustainibility* **2020**, *12*, 6678–6687.
4. Michalik, M; Wilczynska-Michalik, W. Mineral and chemical composition of biomass ash. Proceedings of the European Mineralogical Conference Vol. 1, Frankfurt, Germany, September 2-6 2012; EMC2012-423-1.
5. Kalembkiewicz, J.; Galas, D.; Sitarz-Palczak, E. The Physicochemical Properties and Composition of Biomass Ash and Evaluating Directions of its Applications. *Pol. J. Environ. Stud.* **2018**, *27*, 2593–2603.
6. Zając, G.; Szyszlak-Bargłowicz, J.; Gołębiowski, W.; Szczepanik, M. Chemical Characteristics of Biomass Ashes. *Energies* **2018**, *11*, 2885–2899.
7. Obenberger, L.; Supancic K. Possibilities of ash utilization from biomass combustion plants. Proceeding of the 17th European Biomass Conference and Exhibition, Hamburg, Germany, June/July 2009; Renewable Energies, Eds.; Italy; 2373–2384.
8. Carević, I.; Štirmer, N.; Trkmić, M.; Kostanić Jurić, K. Leaching Characteristics of Wood Biomass Fly Ash Cement Composites. *Appl. Sci.* **2020**, *10*, 8704.
9. Wang, S.; Baxter, L. Comprehensive study of biomass fly ash in concrete: Strength, microscopy, kinetics and durability. *Fuel Process. Technol.* **2007**, *88*, 1165–1170.
10. Salvo, M.; Rizzo, S.; Caldirola, M.; Novajra, G.; Canonico, F.; Bianchi, M.; Ferraris, M. Biomass ash as supplementary cementitious material (SCM). *Adv. Appl. Ceram.* **2015**, *114*, S3-S10.
11. Cabrera, M.; Díaz-López, J.L.; Agrela, F.; Rosales, J. Eco-Efficient Cement-Based Materials Using Biomass Bottom Ash: A Review. *Appl. Sci.* **2020**, 10, 8026.
12. Rajamma, R.; Ball, R.J.; Tarelho, LA.C.; Allen, G.C.; Labrincha, J.A.; Ferreira, V.M. Characterization and use of bio-mass fly ash in cement-based materials. *J. Hazard. Mater.* **2009**, *172*, 1049-1060.
13. Sun, L.; Gong, K. Silicon-Based Materials from Rice Husks and Their Applications. *Ind. Eng. Chem. Res.* **2001**, *40*, 5861–5877.
14. Soltani, N.; Bahrami, A.; Pech-Canul, M.I.; González, L.A. Review on the physicochemical treatments of rice husk for production of advanced materials. *Chem. Eng. J.* **2015**, *264*, 899–935.
15. Zajac, G.; Szyszlak-Bargłowicz, J.; Gołebiowski, W.; Szczepanik, M. Chemical Characteristics of Biomass Ashes. *Energies* **2018**, *11*, 2885.
16. Demirbaş, A. Heavy metal contents of fly ashes from selected biomass samples. *Energy Sources* **2005**, *27*, 1269–1276.
17. Boström, C.E.; Gerde, P.; Hanberg, A.; Jemstrom, B.; Johansson, C.; Kyrkslund, T.; Ranung, A.; Tomqvist, M.; Victorin, K.; Westerholm, R. Cancer risk assessment, indicators, and guidelines for polycyclic aromatic hydrocar-bons in the ambient. *Environ Health Perspect.* **2002**, *110*, 451–488.
18. Baird, W.M.; Hooven, L.A.; Mahdevan, B. Carcinogenic polycyclic aromatic hydrocarbon-DNA adducts and mechanism of action. *Environ. Mol. Mutagen.* **2005**, *2-3*, 106-114.
19. Haykırı-Açma, H. Combustion characteristics of different biomass materials. *Energy Convers. Manag.* **2003**, *44*, 155–162.
20. Cai, J.; He, Y.; Yu, X.; Banks, S.W.; Yang, Y.; Zhang, X.; Yu, Y.; Liu, R.; Bridgwater, A.V. Review of physicochemical properties and analytical characterization of lignocellulosic biomass. *Renew. Sustain. Energy Rev.* **2017**, *76*, 309–322.
21. Hasler, P.; Nussbaumer, T. Particle size distribution of the fly ash from biomass combustion. Proceedings of Biomass for energy and industry, 10th European Conference and Technology Exhibition, Wurzburg, Germany, June 8-11 1998.
22. Rietveld, H.M. A profile refinement method for nuclear and magnetic structures *J. Appl. Cryst.* **1969**, *2*, 65–71.
23. Larson A.C.; Von Dreele R.B. Generalized Structure Analysis System (GSAS) 2000 LANSCE, MS-H805 Los Alamos National Laboratory Los Alamos, NM 87545.
24. Toby, B.H. EXPGUI, a graphical user interface for GSAS. *J. Appl. Crystallogr.* **2001**, *34*, 210–213.
25. Comodi, P.; Nazzareni, S.; Perugini, D. Technology and Provence or roman ceramics from Scoppieto, a mineralogical and petrological study. *Period. di Mineral.* **2006**, *75*, 95–111.
26. Frondini, F.; Zucchini, A.; Comodi, P. Water-rock interaction and trace elements distribution in dolomite aquifers: The Sassolungo and Sella system (Northern Italy). *Geochem. J.* **2014**, *48*, 231–246.
27. Saddique, U.; Muhammad, S.; Tariq, M.; Zhang, H.; Arif, M.; Isthtiaq, A.K.; Khattak, N.U. Potentially toxic elements in soil of the Khyber Pakhtunkhwa province and Tribal areas, Pakistan: evaluation for human and ecological risk. *Environ. Geochem. Health* **2018**, *40*, 2177–2190.
28. Palansooriya, K.N.; Shaheen, M.S.; Chen, S.S.; Tsang, D.C.W.; Hashimoto, Y.; Hou, D.; Bolan, N.S.; Rinklebe, J., Ok, Y.S. Soil amendments for immobilization of potentially toxic elements in contaminated soils: A critical review. *Environ. Int.* **2020**, 134, 105046.
29. ur Rehman, I.; Ishaq, M.; Ali, L.; Muhammad, S., Ud Din, I., Yaseen, M.; Ullah, H. Potentially toxic elements' occurrence and risk assessment through water and soil of Chitral urban environment, Pakistan: a case study. *Environ. Geochem. Health* **2020**, *42*, 4355–4368
30. Schulzke, T. Biomass gasification: conversion of forest residues into heat, electricity and base chemicals. *Chem. Pap.* **2019**, *73*, 1833–1852.

 doi:10.20944/preprints202105.0209.v1

31. Bell, F.G. Lime stabilization of clay minerals and soils. *Eng. Geol.* **1996**, *42*, 223–237.
32. Al-Mukhtar, M.; Lasledj, A.; Alcover, J.F. Behaviour and mineralogy changes in lime-treated expansive soil at 20 °C. *Appl. Clay Sci.* **2010**, *50*, 191–198.
33. Guidobaldi, G.; Cambi, C.; Cecconi, M.; Comodi, P.; Deneele, D.; Paris, M.; Russo, G.; Vitale, E.; Zucchini, A. Chemo-Mineralogical evolution and microstructural modifications of a lime treated pyroclastic soil. *Eng. Geol.* **2018**, *245*, 333–343.
34. Vitale, E.; Russo, G.; Dell'Agli, G.; Ferone, C.; Bartolomeo, C. Mechanical behaviour of soil improved by alkali activated binders. *Environments* **2017**, *4*, 80.
35. Rowe, E.; Withers, A.J.; Baas, P.; Chan, N.; Doody, D.; Holiman, J.; Jacobs, B.; Li, H.; MacDonald, G.K.; McDowell, R.; Sharpley A.N.; Shen, J.; Taheri, W.; Wallenstein, M.; Weintraub, M.N. Integrating legacy soil phosphorus into sustainable nutrient management strategies for future food, bioenergy and water security. *Nutr. Cycling Agroecosyst.* **2016**, *104*, 393–412.